UCLA
UCLA Previously Published Works

Title
An Arctic-Tibetan Connection on Subseasonal to Seasonal Time Scale

Permalink
https://escholarship.org/uc/item/9vx2v42d

Journal
Geophysical Research Letters, 46(5)

ISSN
0094-8276

Authors
Zhang, Yang
Zou, Tao
Xue, Yongkang

Publication Date
2019-03-16

DOI
10.1029/2018gl081476

Peer reviewed

eScholarship.org Powered by the California Digital Library
University of California

Geophysical Research Letters

RESEARCH LETTER
10.1029/2018GL081476

An Arctic-Tibetan Connection on Subseasonal to Seasonal Time Scale

Yang Zhang[1], **Tao Zou**[1], **and Yongkang Xue**[2,3]

[1]CMA-NJU Joint Laboratory for Climate Prediction Studies, Institute for Climate and Global Change Research, School of Atmospheric Sciences, Nanjing University, Nanjing, China, [2]Department of Geography, University of California, Los Angeles, CA, USA, [3]Department of Atmospheric and Oceanic Sciences, University of California, Los Angeles, CA, USA

Key Points:
- Spring surface air temperature in Tibetan Plateau is found significantly linked to the February atmospheric circulation via snow anomaly
- When general circulation is in a combined AO+ and WP- pattern in February, wave trains from Arctic propagate via north and south paths reaching Tibet
- The resultant snow anomaly affects spring surface temperature in Tibetan Plateau, suggesting an Arctic-Tibetan connection on S2S time scale

Correspondence to:
Y. Zhang,
yangzh@alum.mit.edu

Citation:
Zhang, Y., Zou, T., & Xue, Y. (2019). An Arctic-Tibetan connection on subseasonal to seasonal time scale. *Geophysical Research Letters*, *46*. https://doi.org/10.1029/2018GL081476

Received 28 NOV 2018
Accepted 13 FEB 2019
Accepted article online 19 FEB 2019

Abstract Recent research indicates the great potentials of springtime land surface temperature (LST) as a new source of predictability to improve the subseasonal to seasonal climate prediction. In this study, we explore the initial cause of the springtime large-scale LST in Tibetan Plateau (TP) and disentangle its close connection with the February wave activities from the Arctic region. Our Maximum Covariance Analysis show that the spring LST in TP is significantly coupled with the regional snow cover in the preceding months. The latter is further strongly coupled with the February atmospheric circulation and wave activities in mid-to-high latitudes. When the atmospheric circulation is in a combined pattern of Arctic Oscillation and West Pacific teleconnection pattern, wave trains from the Arctic can propagate and reach the TP through northern and southern pathways. This brings dynamical and moisture conditions for the TP snowfall and builds a bridge for Arctic-Tibetan connection.

Plain Language Summary Subseasonal to seasonal prediction, especially the prediction of extreme events as droughts and floods, is one of the major challenges of climate predictions. Recent research suggests the great potentials of springtime land surface temperature (LST) as a new source of predictability to improve subseasonal to seasonal prediction. This study explores the initial cause of the springtime LST anomaly in Tibetan Plateau (TP), through which its close connection with the wintertime wave activities from the Arctic region is discovered. We find that the wave trains from the Arctic can propagate and reach the TP through northern and southern paths, which favors the snowfall in Tibet. The resultant snow anomaly in late winter further affects the springtime LST in TP, which is suggested to be a predictor for the droughts and floods events in Asian monsoon region in early summer. Given the strong influence of TP on the climate variability and water resources in Asian region, our new finding further implies the much broader and long-lasting impacts of Arctic changes on the Asian climate and ecosystem, which has not been comprehensively explored and deserves future studies.

1. Introduction

Subseasonal to seasonal (S2S) prediction, especially the prediction of extreme climate events such as droughts and floods, is one of the major challenges of climate predictions and is the topic of a joint research project of the World Climate Research Program and World Weather Research Program. To improve forecast skills at S2S time scale, it is important to have comprehensive understanding of climate variabilities at this time range and identify important sources of predictability. The connection between the sea surface temperature (SST) and the associated predictability (e.g., the Madden-Julian Oscillation and the evolution of El Niño–Southern Oscillation) has been extensively studied (e.g., Lin et al., 2010; Ting & Wang, 1997; Trenberth et al., 1988; Vitart, 2009; Vitart et al., 2017). Despite its significant prediction value, prediction skill for precipitation anomalies in spring and summer months has remained stubbornly low for years. Many studies consistently show that SST only explains part of the climate variability and predictability at S2S time scale (Pu et al., 2016; Scaife et al., 2009; Schubert et al., 2009; Xue, De Sales, et al., 2016; Xue, Oaida, et al., 2016). Beyond the SST's influence, new mechanisms contributing to the S2S variabilities need to be identified to improve the skills of S2S prediction.

Recent research indicates that springtime land surface temperature (LST) associated with snow anomaly could be a new aspect to improve the climate prediction at S2S time scale. The relationship between the snow in Himalaya/Tibetan Plateau (TP) and the Asian monsoon variability has been identified for decades

©2019. The Authors.
This is an open access article under the terms of the Creative Commons Attribution-NonCommercial-NoDerivs License, which permits use and distribution in any medium, provided the original work is properly cited, the use is non-commercial and no modifications or adaptations are made.

(e.g., Yasunari et al., 1991; Zhang & Zhou, 2015). The snow in North America is also found correlated with the regional droughts and flood events (e.g., Gutzler & Preston, 1997). However, the subsequent studies showed that the effects of the snow cover on summer precipitation are highly variable (e.g., Bamzai & Shukla, 1999; Liu & Yanai, 2002; Wu & Qian, 2003; Xiao & Duan, 2016; Xue et al., 2012), suggesting the difficulty of using snow in TP directly as a predictor for droughts and flood events. Studies by Xue, Oaida, et al., (2016) and Xue et al. (2018) therefore conjectured that a temporally filtered response to the snow anomalies may be preserved in the LST and found that, in both North America and East Asia, the springtime large-scale LST anomalies all significantly affect the early summer precipitation in its downstream region. Their observational analysis show that the connections between the LST and its downstream summer precipitation are as significant as the well-known SST-precipitation connections. Modeling studies of the two regions further show the driving effects of the LST in west Unite States and the TP to their downstream flood/drought in the following month, suggesting the great potentials of LST as a new source of predictability for S2S prediction.

Though observational and modeling studies illustrate the downstream impacts of LST to the drought and flood events, many questions remain to further explore this new approach. One of the important questions is the initial cause for the large-scale LST anomalies, especially its relation with the snow. The conjecture on the relationship between the land temperature and the preceding snow anomalies still needs to evaluate with the observational evidence. Current modeling studies reveal the LST impacts with 1 month lead; however, it remains an open question as to whether longer lead time of the LST or the other closely related fields exhibit potential predictability as well. In this study, the above issues are investigated in the TP-Asian monsoon region. By comparing and analyzing multiple observational data set, this study shows that the springtime (April and May) LST in TP is strongly coupled to the snow cover days in the region and is further significantly linked to the extratropical atmospheric circulation in February. When the February circulation is in a combined mode of Arctic Oscillation (AO) and West Pacific (WP) teleconnection patterns (Wallace & Gutzler, 1981), strong wave trains originated from the Arctic emerge and propagate through northern and southern paths far-reaching the Tibet, providing dynamical and moisture conditions for the TP snowfall. The resultant snowfall thus snow cover anomalies can further affect the spring LST in the region, suggesting a mechanism for Arctic-Tibetan connection on S2S time scale.

2. Data and Methodology

Multiple data sets are applied and compared to investigate the connections between LST and snow in TP, as well as large-scale atmospheric circulation, and to evaluate the results' robustness. Since there are no long-term large-scale LST observations that can be used to produce climatology, monthly 2-m surface air temperature (T-2m) is used for this analysis as in Xue et al. (2018). The soundness for this substitution is supported by ensemble simulations with multiple global and regional climate models, in which the LST was imposed as initial conditions and produced the observed T-2m. The T-2m data used in the study are from the National Oceanic and Atmospheric Administration (NOAA) Climate Anomaly Monitoring System (CAMS, Ropelewski et al., 1985; Fan & Van den Dool, 2008) near-surface 2-m air temperature station data from year 1973 to 2014 and the China Ground 2-m Temperature and Precipitation Grid Dataset (V2.0) at 0.5° × 0.5° spatial resolution produced by the National Meteorological Information Center of the China Meteorological Administration (National Meteorological Information Center, 2012). The atmospheric circulation data apply the monthly National Centers for Atmospheric Prediction-National Center for Atmospheric Research (NCEP-NCAR) reanalysis (Kalnay et al., 1996) compiled on a spatial resolution of 2.5° × 2.5° regular latitude-longitude grid. The ERA-Interim reanalysis data set (Dee et al., 2011) with a 1.0° × 1.0° spatial resolution is also checked to confirm the results. The precipitation data apply the daily APHRODITE data set (Yatagai et al., 2012). The precipitation data of Global Precipitation Climatology Centre (GPCC) Full Data Version 7 (Schneider et al., 2016) are also compared to confirm the results. The above comparisons all show similar results and thus will not be shown. The relative humidity applies the National Aeronautics and Space Administration MERRA-2 monthly data (Gelaro et al., 2017). The data of snow cover days from 101 station observations in TP from year 1973 to 2014 are also used in the study (Zhao et al., 2007). The snow data sets include the snow coverage and snow depth. Our analyses show that only snow cover days present statistical significant results with other variables and will be discussed in this paper.

The Maximum Covariance Analysis (MCA, also called singular value decomposition analysis; Bretherton et al., 1992; Gu et al., 2018; Wallace et al., 1992; Xue et al., 2005) is conducted between the springtime (April and May average) T-2m and the earlier month snow coverage in the TP, as well as the earlier month 200-hPa

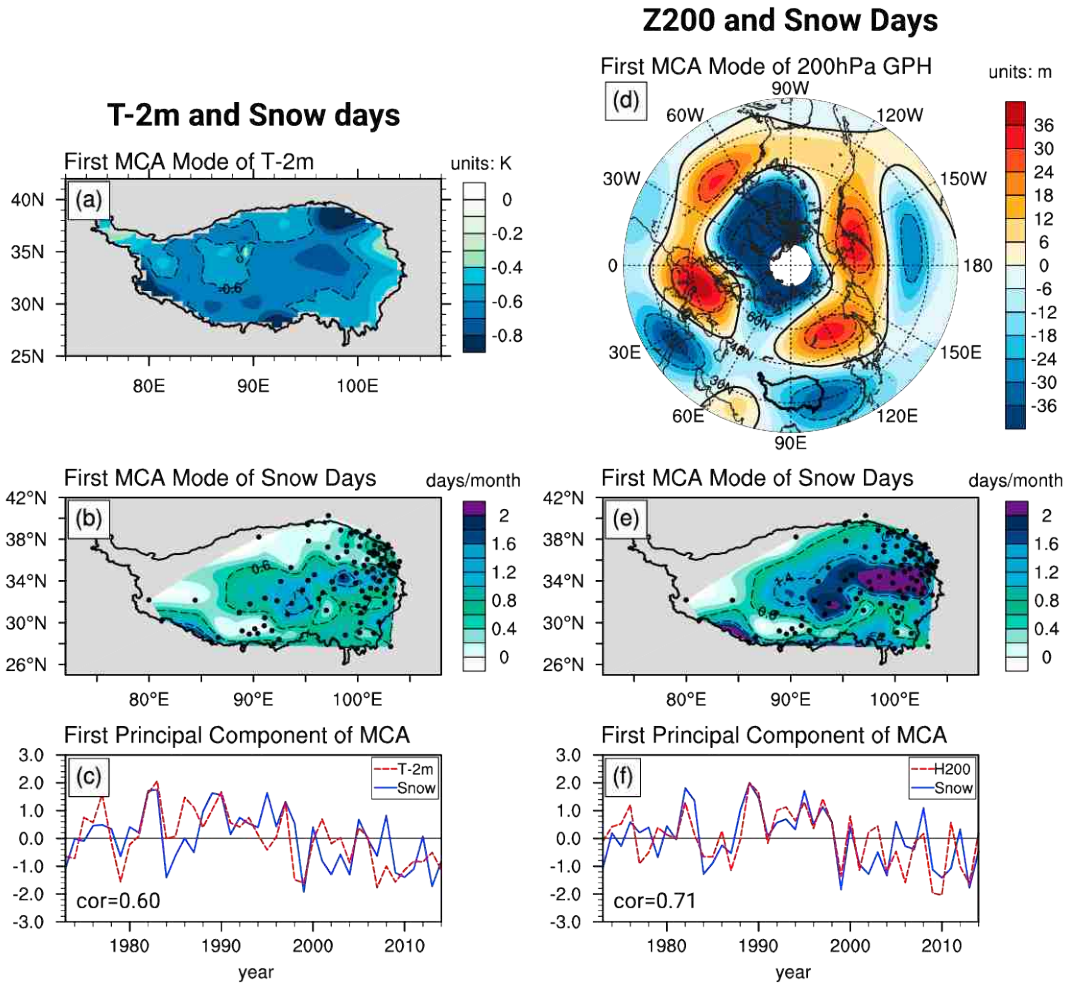

Figure 1. (a–c) First coupled MCA mode between (a) April–May (AM) averaged 2-m temperature and (b) February to April (FMA) averaged snow cover days, and (c) their corresponding standardized principal components. The squared covariance fraction of the mode is 82.5%. The correlation between the two fields is 0.6. (d–f) Same as (a)–(c), respectively, but between February 200-hPa geopotential height and FMA snow cover days over Tibetan Plateau. Squared covariance fraction of the first mode is 62.4%. The correlation between the two fields is 0.71. Spatial patterns in (b) and (d) are presented as homogeneous regression maps to display the spatial localization of their covarying part. Spatial patterns in (a) and (e) are presented as heterogeneous regression maps to relate their changes to the variations of Tibetan Plateau snow in panel (b) and Z200 in panel (d) in preceding months, respectively. Contour intervals are 0.1 K in panel (a), 0.2 days/month in panels (b) and (e), and 6 m in panel (d). Both of the MCA modes are significant above the 99% confidence level by Monte Carlo test with 1,000 ensemble simulations. T-2m = 2-m surface air temperature; MCA = Maximum Covariance Analysis; GPH = geopotential height.

geopotential height over the north of 20°N to detect the precursor signals responsible for the TP snow and springtime LST anomalies. Through the singular value decomposition of the covariance matrix between springtime T-2m and earlier time monthly 200-hPa geopotential height, their coupled spatial patterns and their temporal variations can be identified. The Monte Carlo test (Iwasaka & Wallace, 1995) is applied to all the MCA results presented in this paper by performing a thousand ensembles of MCA analysis, in which the T-2m field is kept fixed while the field of geopotential height is randomly disordered in time. The significance can be estimated by sorting the results of MCA ensembles and comparing the observed MCA statistics with the ensemble simulations. In this study, we investigate the first MCA modes whose significances exceed 99% confidence level, which suggests a robust and dominant linkage between two fields.

3. Results

3.1. MCA Results

MCA analyses are first applied for the April–May averaged T-2m field in TP and the snow anomaly as well as circulation fields in previous months to detect the significant factors affecting the springtime LST. Our

analyses find that the most significant related field to T-2m is snow cover days in TP in previous months. As shown in Figures 1a and 1b, the first MCA mode for T-2m exhibits pronounced anomaly pattern over the whole TP, especially over the eastern and central TP region. Coupled with the cold anomalies in T-2m field, the snow cover days in the previous February, March, and April (FMA) in the region are significantly increased, especially in the eastern part of the TP. Results are similar and robust if only the snow cover days in a single month, such as February, March, or April, are used (not shown). This mode accounts for 82.5% of the total covariance between the two fields, with their correlation reaches 0.60 as shown in Figure 1c.

To understand the cause of change in TP snow cover in FMA, MCA analysis is further conducted between the snow cover days in FMA and 200-hPa geopotential height (Z200) in previous winter. The results of the MCA analysis show that the snow cover days in TP region in the early spring is significantly coupled with the large-scale atmospheric circulation pattern in February. As shown in Figures 1d and 1e, the increase in the snow cover days in TP is strongly linked to a meridional tripole anomalous pattern in the field of geopotential height in February, with evident action centers above the Arctic, northern Eurasia, and the south of TP. This mode accounts for 62.4% of the total covariance between the two fields, with their correlation coefficients reaches 0.71 as shown in Figure 1f. The time series of the snow cover days in Figure 1f is highly correlated with that in Figure 1c, which is as high as 0.985, representing the same events in Figures 1b and 1e. The same Z200 circulation pattern as that in Figure 1d can be obtained if regression analyses are directly conducted upon the time series of TP snow cover days in Figure 1c or 1f (not shown). Therefore, the two groups of MCA results imply a robust connection between the springtime LST in TP region and the February extratropical atmospheric circulations. Such connection is linked by the TP snowfall from late winter to early spring, which suggests that the anomalous extratropical atmospheric circulation in late winter leads to the anomalous snowfall in TP region. Given the high elevation of TP, its wintertime snowfall can accumulate till the season of snow melting, which is April and May, thus has a long-lasting influence on the snow cover as suggested by Shaman and Tziperman (2005) and greatly affects the LST in the region. The mechanism for such connection is further investigated in the following section.

3.2. Mechanisms

Regression analysis is applied to the February 500-hPa geopotential height (Z500) upon the time series of Z200 in the first MCA mode to understand the influence of the February atmospheric circulation on the snowfall in TP region. As shown in Figure 2a, the anomalous pattern of geopotential height at 500 hPa exhibits a meridional dipole structure in middle-to-polar region but with more zonal asymmetry compared to that at 200 hPa in Figure 1d. There are evident negative anomalies at 60°E in northern Eurasia accompanied by the positive anomalies to its west and east, suggesting an enhanced trough near the Ural region, which favors the southward movement of the wintertime cold air. In the subtropical belt, negative anomalies at Z500 present expanding from west Asia, south of Tibet to the North Pacific.

Such a Z500 pattern in Figure 2a actually denotes a combined effect of AO and WP teleconnection patterns. AO and WP are the leading patterns of variability of the large-scale atmospheric circulation over middle-to-high latitudes of the Northern Hemisphere and over the North Pacific, respectively, whose phases have great impacts on the weather and climate over those regions (Barnston & Livezey, 1987; Thompson & Wallace, 1998; Wallace & Gutzler, 1981). Their spacial patterns in terms of Z500 are plotted in Figures 2b and 2c by conducting the regressions upon the AO and WP indices provided by the NOAA Climate Prediction Center. The detailed calculations of AO and WP indices can be found from Climate Prediction Center website (https://www.cpc.ncep.noaa.gov/data/teledoc/telepatcalc.shtml). Comparing with the individual AO or WP patterns, the Z500 pattern associated with the first MCA mode represents a typical AO pattern in its positive phase with action centers in the Arctic-Atlantic sector. In the East Asia-North Pacific sector, the Z500 pattern with the MCA1 mode represents a typical WP pattern in its negative phase not only with action centers in the northeast Asia and middle-to-high latitudes North Pacific, overlapped with the AO pattern, but also a strong action center in the subtropical belt from the south of TP to the North Pacific. The sum of the Z500 patterns of AO+ and WP− thus is also plotted in Figure 2d to compare with Figure 2a. All the above results show that the Z500 pattern in the first MCA mode is mostly the combination of the February AO and WP patterns, with strong action centers expanding from the Arctic-Atlantic to the East Asia-North Pacific regions.

Besides the spatial pattern, temporal relations between the first MCA mode and the AO and WP are also investigated. Figure 2e plots the variations of the time series of Z200 in the first MCA mode and the indices of

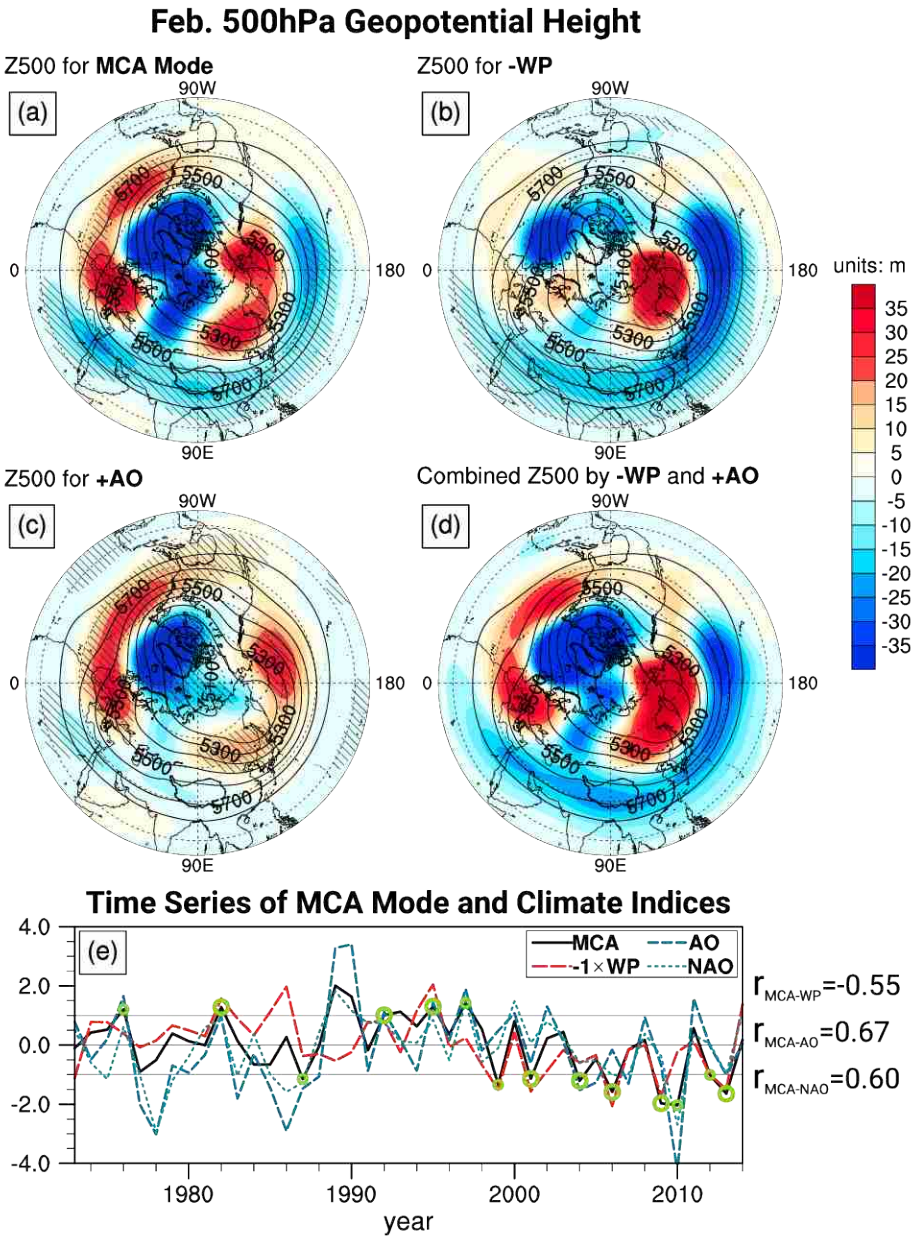

Figure 2. Regression patterns of 500-hPa geopotential height in February upon the standardized times series of (a) 200-hPa geopotential height in the first MCA mode, (b) (−1) × WP index and (c) AO index. (d) The sum of the patterns in (b) and (c). Color shading interval is 5 m in panels (a)-(d). The stripe-shaded regions denote values above the 95% confidence level by *F* test (von Storch & Zwiers, 2002). In panels (a)–(d), the climatology of 500-hPa geopotential height is also plotted in black contours for comparison. (e) Year-by-year variations of the time series of Z200 in the first MCA mode and indices of February (−1)×WP and AO. Typical MCA1 mode (stronger than ±1 standard deviation) that occurs in the year of AO+ and WP− (or AO− and WP+) is marked with green circles. In panel (e), time series of North Atlantic Oscillation (NAO) is also plotted, which can reflect the oscillation of AO in the North Atlantic-Arctic sector. The WP, AO, and North Atlantic Oscillation indices are downloaded from National Oceanic and Atmospheric Administration Climate Prediction Center (NOAA). MCA = Maximum Covariance Analysis; WP = West Pacific; AO = Arctic Oscillation.

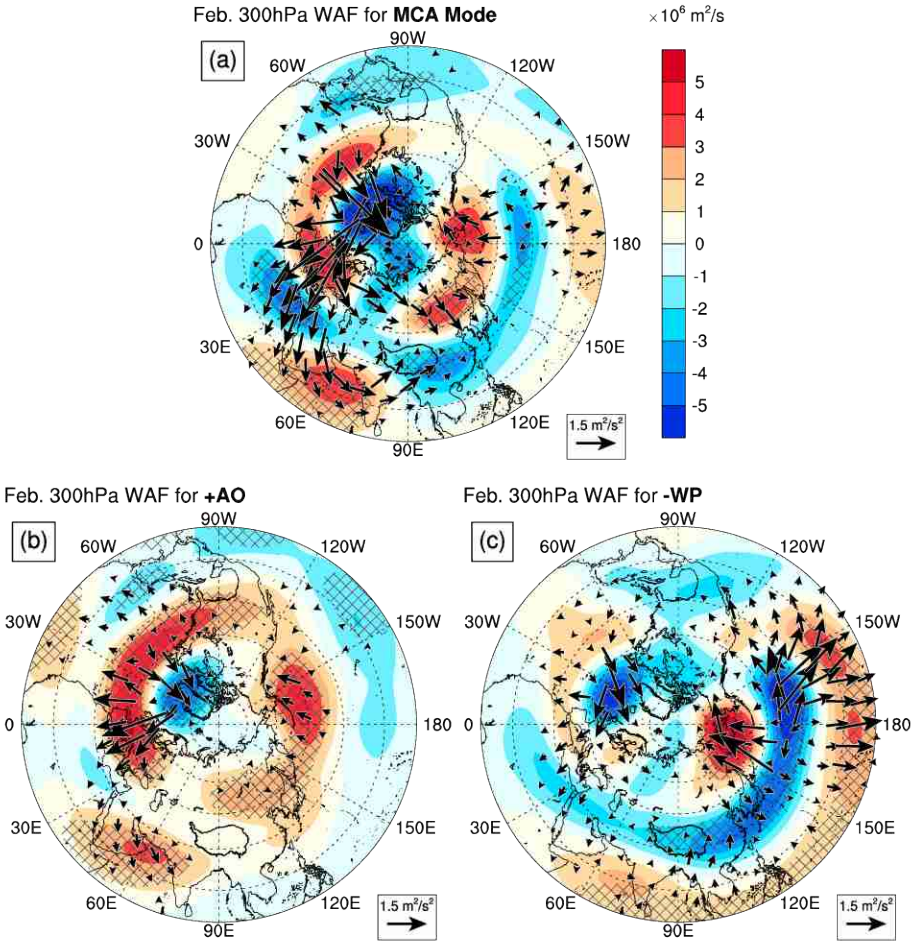

Figure 3. Regressed patterns of 300-hPa stream function (calculated from the horizontal winds, color shading) and corresponding wave activity flux of TN01 (arrows, unit: m^2/s^2) upon the standardized times series of (a) 200-hPa geopotential height in the first MCA mode, (b) AO indices, and (c) (−1) × WP indices. Cross-hatching regions indicate values exceeding 95% confidence level by *F* test (von Storch & Zwiers, 2002). MCA = Maximum Covariance Analysis; WP = West Pacific; AO = Arctic Oscillation.

AO and WP. As shown in the figure, most of the typical (stronger than ±1 standard deviation) MCA1 mode in Figure 2a occurs in the situation that AO+ and WP− (or AO− and WP+) emerge at the same time. Such relationship becomes even more evident since the mid-1990s. Correlations between the time series of MCA1 mode and AO, WP indices are also calculated. The temporal correlations between the MCA1 time series and the February monthly AO/WP indices are 0.67/−0.55, respectively. A bivariate regression model (von Storch & Zwiers, 2002) for the MCA1 time series with respect to the AO and WP indices is also constructed to further quantify their relationship. In the regression model, the two indices explain up to 78.6% of the total variance of the Z200 time series, which again shows that the variability of the atmospheric circulation in the MCA1 mode mostly denotes a combined effect of February AO and WP teleconnection patterns.

Regression analysis is further applied on the upper tropospheric wave activity flux (WAF) to understand why such a combined pattern, instead of the single AO or WP pattern, is strongly coupled with the late winter snowfall in TP. The WAF derived by Takaya & Nakamura (2001, hereafter TN01) is used to quantify the wave energy propagation in accordance with the background flow. It can explicitly delineate the propagation of wave energy in a zonally varying basic flow, with its direction parallel to the local three-dimensional group velocity of Rossby waves. Given the low tropopause in the polar region, here we plot the 300-hPa WAF instead of 200 hPa to avoid the influence. The WAF in Figure 3 helps delineate the strong coupling between the TP snowfall and the combined atmospheric circulation pattern. With the combined pattern, as shown in Figure 3a, the WAF exhibits two evident branches of wave trains originating from the Arctic regions and encountering at the TP, providing necessary dynamical conditions for the anomalous February

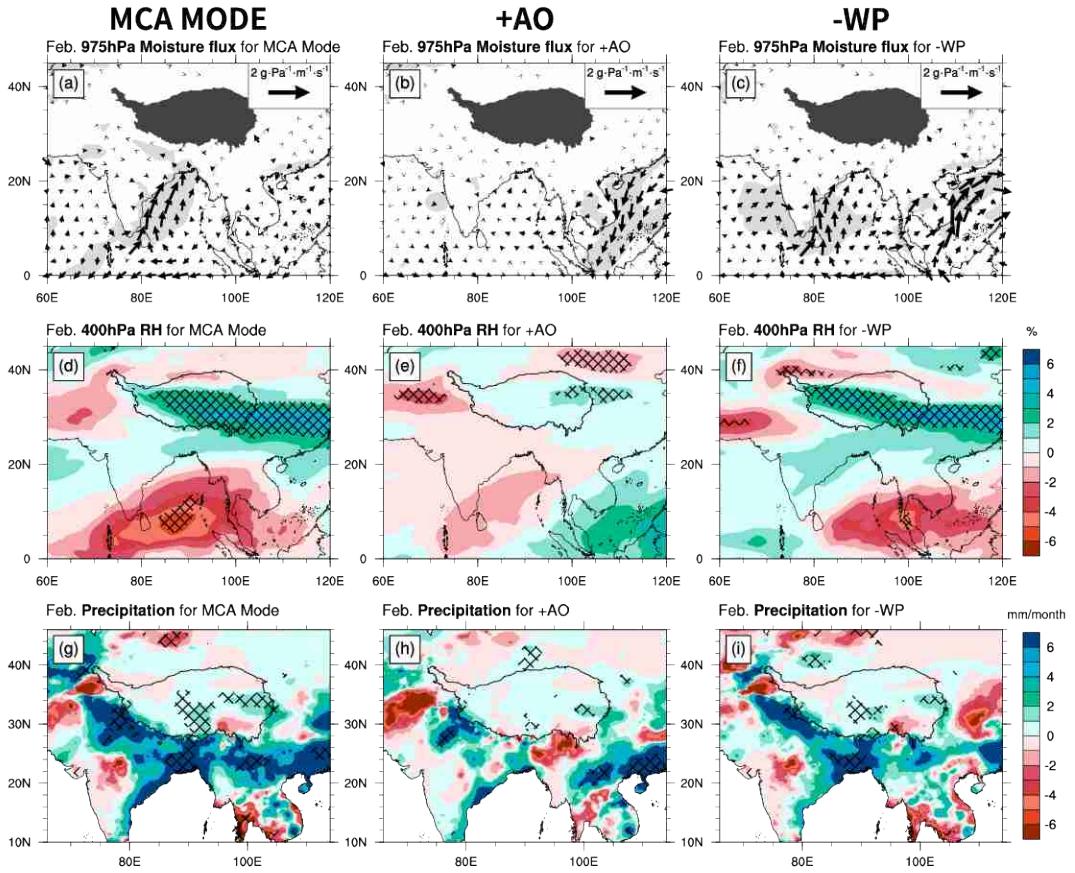

Figure 4. Regression patterns of February 975-hPa moisture flux (unit: $g{\cdot}Pa^{-1}{\cdot}m^{-1}\cdot s^{-1}$, denoting mass flux of water vapor per unit area and time) upon the standardized times series of (a) 200-hPa geopotential height in the first MCA mode, (b) AO indices, and (c) $(-1)\times$ WP indices. (d–f) Same as (a)–(c), respectively, but for February 400-hPa relative humidity (%). (g–i) Same as (a)–(c), respectively, but for the precipitation in February using APHRODITE data set (unit: mm/month). In panels (a)–(c), gray shaded region denotes values exceeding 95% confidence level by *F* test. In panels (d)–(i), crossed region denotes values exceeding the 95% confidence level by *F* test (von Storch & Zwiers, 2002). MCA = Maximum Covariance Analysis; WP = West Pacific; AO = Arctic Oscillation; RH = relative humidity.

precipitation around the TP region (mostly the snowfall). The southern branch of the wave train originates from the Arctic Iceland and Norwegian Sea, with the wave energy propagating southeastward through the European continent to the warm and moist Arabian Sea and Bay of Bengal, finally reaches the south slope of TP, which favors the moisture supply from Bay of Bengal up to the TP. The northern branch of the wave train originates from the Scandinavia and Arctic Barents and Kara Seas and propagates to the north of China reaching the north TP slope, which benefits the invasion of the northern cold air to the TP. The cold air invasion can help increase the relative humidity in the TP, which favors the wintertime snowfall in the region as well. The regressions of the WAF upon the AO and WP index in Figures 3b and 3c show that neither the AO nor WP pattern alone can support such long-reaching wave trains that affect the TP snowfall. With the AO signal alone, the upstream wave train can propagate southward through the European continent but becomes weaker and cannot propagate downstream any further through the Arabian Sea and Bay of Bengal to reach the south slope of TP. Only with the support of the downstream WP pattern can the upstream AO signals reach the TP. The same situation also happens to the northern branch of the wave train, which only appears in the combined pattern.

The regression analyses on the moisture transport, relative humidity, and the precipitation further show the combined effect of AO and WP signals on the TP snow anomalies. As shown in Figure 4, in the MCA mode, the low-level moisture flux (defined as $\frac{1}{g}q\vec{v}$, where q is specific humidity, g is acceleration due to gravity, and $\vec{v}$ is horizontal wind) exhibits evident moisture transport from Bay of Bengal to TP. Such moisture transport is absent in an individual positive AO event and appears in the negative phase of WP but with

weaker amplitude and not extending into the TP as in the MCA mode. Thus, the WP pattern of atmospheric circulation in the Asia-Pacific sector extends the wave train exaggerated in the AO event further downward to the TP and enhances the moisture supply there. The regressions of relative humidity in Figures 4d–4f show that both the WP and AO acts to enhance the relative humidity in the TP region, with the relative humidity in WP pattern enhanced much stronger. In the combined pattern, the relative humidity gets most strong enhancement, stronger than the sum of the enhancement in individual AO and WP pattern, implying an amplification with the combined signals. The regressions of precipitation with the MCA mode in Figure 4g show a consistent enhancement, especially in the south slope as well as the center and the east of TP, a pattern similar to that with the WP pattern in Figure 4i. All of the above analysis show that, in a combined pattern of AO and WP, the wave trains from the Arctic region can propagate onto the TP region, providing dynamical and moisture conditions for the regional snowfall.

It is worthy of note that AO and WP are not only the leading modes of internal intraseasonal variabilities (e.g., Linkin & Nigam, 2008; Lorenz & Hartmann, 2003; Nie et al., 2013; Zhang et al., 2012) but also the preferred response pattern of the extratropical atmosphere to the external forcing on longer time scales (e.g., Ring & Plumb, 2007). Many studies have suggested that the Arctic warming can induce AO-like atmospheric response (e.g., Butler et al., 2010; Nie et al., 2016). Variations of AO and WP are closely related to the change of sea ice (e.g., Linkin & Nigam, 2008; Overland et al., 2015) as well as the SST anomalies in extratropical and tropical oceans (e.g., Kwon et al., 2010; Xiao et al., 2016). The latter is suggested influence the TP snowfall by modulating the moisture supply as well (Yuan et al., 2009, 2012). How the atmospheric circulation pattern in the MCA1 mode links to those external forcing is an important topic that needs further investigation. Though this study identifies the significant connection between the February atmospheric circulation and the TP spring LST via the snow anomaly, further diagnosis and modeling studies are still needed to disentangle the detailed land-snow-atmosphere interactions in the TP to fully understand the mechanism of the connection.

4. Summary and Discussion

Recent research indicates the potentials of LST as a new source of predictability, complementing SST signals, to improve the S2S prediction. This study investigates the initial causes of the large-scale TP LST anomalies in springtime and disentangles its close linkage to the February wave activity propagating from the Arctic region. Our MCA analyses show that the spring LST is significantly coupled with the regional snow cover in preceding months. This provides observational evidence to the conjecture in Xue et al. (2018) that a temporally filtered response to snow anomalies is preserved in the LST memory, with the latter a more effective predictor to drought and flood events. The TP region snow cover can further originate back to the anomalous atmospheric circulation in middle and high latitudes in February, suggesting that the February anomalous circulation, through the resultant anomalies in snowfall in late winter and snow cover in early spring in TP region, can eventually lead to large-scale anomalies in LST in spring time.

Our diagnosis further show that the anomalous atmospheric circulation coupled to the TP LST essentially denotes a combined mode of AO and WP teleconnection pattern. The AO is known as the dominant mode of variability of the extratropical large-scale atmospheric circulation. Our analyses show that, only with the proper circulation pattern in the downstream East Asia-North Pacific region, the AO can have significant influence in TP. When the atmospheric circulation in Arctic-Atlantic sector presents the positive phase of AO and the East Asia-North Pacific sector presents the negative phase of WP, the two patterns all act to deepen the trough in Ural region, which favors the cold air invasion thus the increase in TP relative humidity. More importantly, only in the combined mode, the wave trains originated from the Arctic can reach the TP through the northern and southern branches. This brings dynamical and moisture conditions for the TP snowfall, building a bridge for Arctic-Tibetan connection.

Recent years, the impacts of Arctic changes on the weather and climate in lower latitudes draw much attentions in scientific community and in the public. Though many possible mechanisms have been proposed for the Arctic-midlatitude linkage (e.g., Francis, 2017; Kim et al., 2014; Wu & Zhang, 2010) and the roles of the southward propagation of wave trains from the Arctic region have been emphasized for the linkage (Gu et al., 2018; Overland et al., 2015), the effects of Arctic on the weather and climate in TP has not been comprehensively investigated. Given the strong influence of the TP on Asian monsoon variabilities and the interactions between the TP snow and the Indian Ocean SST (Yuan et al., 2018, 2012), our study suggests that the Arctic wave activity may have a much broader and long-lasting impacts on the lower latitudes by affecting

the snow thus the springtime LST in the TP. Whether the Arctic amplification in recent decade would play an important role in the changing climate in TP and Asian region, as well as in the tropical ocean, is a topic very deserving further studies. Though this study focuses on the TP, further work will be conducted to apply the initial causes of the large-scale land surface anomalies in North America as well, where the spring LST anomalies have also been shown to have large impact of the North American drought/flood events (Xue et al., 2018; Xue, Oaida, et al., 2016).

Acknowledgments
The authors thank the two anonymous reviewers for their constructive suggestions, which help improve the quality of the manuscript. This study was supported by the National Key Research and Development Program of China under grant 2018YFC1506001, Strategic Priority Research Program of Chinese Academy of Sciences under grant XDA20000000, National Natural Science Foundation of China under grants 41675055 and 41621005, and the grants from U.S. National Science Foundation AGS-1346813 and AGS-1419526. The CAMS gridded 2-m temperature is available at https://www.esrl.noaa.gov/psd/data/gridded/data.ghcncams.html website. The GPCC precipitation is available at https://rda.ucar.edu/datasets/ds496.0 website. The APHRODITE daily precipitation is available at http://search.diasjp.net/en/dataset/APHRO_MA website. The China Ground 2-m Temperature and Precipitation Grid Dataset is available at http://cdc.nmic.cn website. The MERRA relative humidity is downloaded at https://disc.gsfc.nasa.gov/datasets/M2IMNPASM_V5.12.4/summary website. The reanalysis of NCEP-NCAR can be downloaded from https://www.esrl.noaa.gov/psd/data/gridded/data.ncep.reanalysis.pressure.html and the reanalysis of ERA-interim from http://www.ecmwf.int/en/research/climate-reanalysis/era-interim website. Indices of AO and WP are obtained from https://www.esrl.noaa.gov/psd/data/climateindices/list website.

References

Bamzai, A. S., & Shukla, J. (1999). Relation between Eurasian snow cover, snow depth, and the Indian summer monsoon: An observational study. *Journal of Climate*, *12*(10), 3117–3132. https://doi.org/10.1175/1520-0442(1999)012<3117:RBESCS>2.0.CO;2

Barnston, A. G., & Livezey, R. E. (1987). Classification, seasonality and persistence of low-frequency atmospheric circulation patterns. *Monthly Weather Review*, *115*, 1083–1126. https://doi.org/10.1175/1520-0493(1987)115<1083:CSAPOL>2.0.CO;2

Bretherton, C. S., Smith, C., & Wallace, J. M. (1992). An intercomparison of methods for finding coupled patterns in climate data. *Journal of climate*, *5*(6), 541–560. https://doi.org/10.1175/1520-0442(1992)005<0541:AIOMFF>2.0.CO;2

Butler, A. H., Thompson, D. W. J., & Heikes, R. (2010). The steady-state atmospheric circulation response to climate change-like thermal forcings in a simple general circulation model. *Journal of Climate*, *23*(13), 3474–3496. https://doi.org/10.1175/2010JCLI3228.1

Dee, D. P., Uppala, S. M., Simmons, A. J., Berrisford, P., Poli, P., Kobayashi, S., et al. (2011). The ERA-Interim reanalysis: Configuration and performance of the data assimilation system. *Quarterly Journal of the Royal Meteorological Society*, *137*(656), 553–597. https://doi.org/10.1002/qj.828

Fan, Y., & van den Dool, H. (2008). A global monthly land surface air temperature analysis for 1948–present. *Journal of Geophysical Research*, *113*, D01103. https://doi.org/10.1029/2007JD008470

Francis, J. A. (2017). Why are Arctic linkages to extreme weather still up in the air? *Bulletin of the American Meteorological Society*, *98*(12), 2551–2557. https://doi.org/10.1175/BAMS-D-17-0006.1

Gelaro, R., McCarty, W., Suarez, M. J., Todling, R., Molod, A., Takacs, L., et al. (2017). The Modern-Era Retrospective Analysis for Research and Applications, version 2 (MERRA-2). *Journal of Climate*, *30*(14), 5419–5454. https://doi.org/10.1175/JCLI-D-16-0758.1

Gu, S., Zhang, Y., Wu, Q., & Yang, X.-Q. (2018). The linkage between Arctic sea ice and midlatitude weather: In the perspective of energy. *Journal of Geophysical Research: Atmospheres*, *123*, 11,536–11,550. https://doi.org/10.1029/2018JD028743

Gutzler, D. S., & Preston, J. W. (1997). Evidence for a relationship between spring snow cover in North America and summer rainfall in New Mexico. *Geophysical Research Letters*, *24*(17), 2207–2210. https://doi.org/10.1029/97GL02099

Iwasaka, N., & Wallace, J. M. (1995). Large scale air sea interaction in the Northern Hemisphere from a view point of variations of surface heat flux by SVD analysis. *Journal of the Meteorological Society of Japan. Ser. II*, *73*(4), 781–794. https://doi.org/10.2151/jmsj1965.73.4_781

Kalnay, E., Kanamitsu, M., Kistler, R., Collins, W., Deaven, D., Gandin, L., et al. (1996). The NCEP/NCAR 40-Year reanalysis project. *Bulletin of the American meteorological Society*, *77*(3), 437–471. https://doi.org/10.1175/1520-0477(1996)077<0437:TNYRP>2.0.CO;2

Kim, B.-M., Son, S.-W., Min, S.-K., Jeong, J.-H., Kim, S.-J., Zhang, X., et al. (2014). Weakening of the stratospheric polar vortex by Arctic sea-ice loss. *Nature communications*, *5*, 4646. https://doi.org/10.1038/ncomms5646

Kwon, Y.-O., Alexander, M. A., Bond, N. A., Frankignoul, C., Nakamura, H., Qiu, B., & Thompson, L. A. (2010). Role of the Gulf Stream and Kuroshio Oyashio systems in large-scale atmosphere ocean interaction: A review. *Journal of Climate*, *23*(12), 3249–3281. https://doi.org/10.1175/2010JCLI3343.1

Lin, H., Brunet, G., & Fontecilla, J. S. (2010). Impact of the Madden-Julian Oscillation on the intraseasonal forecast skill of the North Atlantic Oscillation. *Geophysical Research Letters*, *37*, L19803. https://doi.org/10.1029/2010GL044315

Linkin, M. E., & Nigam, S. (2008). The North Pacific Oscillation West Pacific teleconnection pattern: Mature-phase structure and winter impacts. *Journal of Climate*, *21*(9), 1979–1997. https://doi.org/10.1175/2007JCLI2048.1

Liu, X., & Yanai, M. (2002). Influence of Eurasian spring snow cover on Asian summer rainfall. *International Journal of Climatology: A Journal of the Royal Meteorological Society*, *22*(9), 1075–1089. https://doi.org/10.1002/joc.784

Lorenz, D. J., & Hartmann, D. L. (2003). Eddy-zonal flow feedback in the Northern Hemisphere winter. *Journal of Climate*, *16*(8), 1212–1227. https://doi.org/10.1175/1520-0442(2003)16<1212:EFFITN>2.0.CO;2

National Meteorological Information Center (2012). Assessment report of China's ground precipitation 0.5 × 0.5 Gridded Dataset (V2. 0).

Nie, Y., Zhang, Y., Chen, G., & Yang, X.-Q. (2016). Delineating the barotropic and baroclinic mechanisms in the midlatitude eddy-driven jet response to lower-tropospheric thermal forcing. *Journal of the Atmospheric Sciences*, *73*(1), 429–448. https://doi.org/10.1175/JAS-D-15-0090.1

Nie, Y., Zhang, Y., Yang, X.-Q., & Chen, G. (2013). Baroclinic anomalies associated with the Southern Hemisphere Annular Mode: Roles of synoptic and low-frequency eddies. *Geophysical Research Letters*, *40*, 2361–2366. https://doi.org/10.1002/grl.50396

Overland, J., Francis, J. A., Hall, R., Hanna, E., Kim, S.-J., & Vihma, T. (2015). The melting Arctic and midlatitude weather patterns: Are they connected? *Journal of Climate*, *28*(20), 7917–7932. https://doi.org/10.1175/JCLI-D-14-00822.1

Pu, B., Fu, R., Dickinson, R. E., & Fernando, D. N. (2016). Why do summer droughts in the Southern Great Plains occur in some La Niña years but not others? *Journal of Geophysical Research: Atmospheres*, *121*, 1120–1137. https://doi.org/10.1002/2015JD023508

Ring, M. J., & Plumb, R. A. (2007). Forced annular mode patterns in a simple atmospheric general circulation model. *Journal of the Atmospheric Sciences*, *64*(10), 3611–3626. https://doi.org/10.1175/JAS4031.1

Ropelewski, C. F., Janowiak, J. E., & Halpert, M. S. (1985). The analysis and display of real time surface climate data. *Monthly Weather Review*, *113*, 1101–1106. https://doi.org/10.1175/1520-0493(1985)113<1101:TAADOR>2.0.CO;2

Scaife, A. A., Kucharski, F., Folland, C. K., Kinter, J., Brönnimann, S., Fereday, D., et al. (2009). The CLIVAR C20C project: Selected twentieth century climate events. *Climate Dynamics*, *33*(5), 603–614. https://doi.org/10.1007/s00382-008-0451-1

Schneider, U., Becker, A., Finger, P., Meyer-Christoffer, A., Rudolf, B., & Ziese, M. (2016). GPCC full data reanalysis version 7.0: Monthly land-surface precipitation from rain gauges built on GTS based and historic data. https://doi.org/10.5065/D6000072

Schubert, S., Gutzler, D., Wang, H., Dai, A., Delworth, T., Deser, C., et al. (2009). A U.S. CLIVAR project to assess and compare the responses of global climate models to drought-related SST forcing patterns: Overview and results. *Journal of Climate*, *22*(19), 5251–5272. https://doi.org/10.1175/2009JCLI3060.1

Shaman, J., & Tziperman, E. (2005). The effect of ENSO on Tibetan Plateau snow depth: A stationary wave teleconnection mechanism and implications for the South Asian monsoons. *Journal of Climate*, *18*(12), 2067–2079. https://doi.org/10.1175/JCLI3391.1

Takaya, K., & Nakamura, H. (2001). A formulation of a phase-independent wave-activity flux for stationary and migratory quasigeostrophic eddies on a zonally varying basic flow. *Journal of the Atmospheric Sciences*, *58*(6), 608–627. https://doi.org/10.1175/1520-0469(2001)058<0608:AFOAPI>2.0.CO;2

Thompson, D. W., & Wallace, J. M. (1998). The Arctic Oscillation signature in the wintertime geopotential height and temperature fields. *Geophysical research letters*, *25*(9), 1297–1300. https://doi.org/10.1029/98GL00950

Ting, M., & Wang, H. (1997). Summertime US precipitation variability and its relation to Pacific sea surface temperature. *Journal of Climate*, *10*(8), 1853–1873. https://doi.org/10.1175/1520-0442(1997)010<1853:SUSPVA>2.0.CO;2

Trenberth, K. E., Branstator, G. W., & Arkin, P. A. (1988). Origins of the 1988 North American drought. *Science*, *242*(4886), 1640–1645. https://doi.org/10.1126/science.242.4886.1640

Vitart, F. (2009). Impact of the Madden Julian Oscillation on tropical storms and risk of landfall in the ECMWF forecast system. *Geophysical Research Letters*, *36*, L15802. https://doi.org/10.1029/2009GL039089

Vitart, F., Ardilouze, C., Bonet, A., Brookshaw, A., Chen, M., Codorean, C., et al. (2017). The subseasonal to seasonal (S2S) prediction project database. *Bulletin of the American Meteorological Society*, *98*(1), 163–173. https://doi.org/10.1175/BAMS-D-16-0017.1

von Storch, H., & Zwiers, F. W. (2002). *Statistical analysis in climate research*. Cambridge, UK: Cambridge University Press.

Wallace, J. M., & Gutzler, D. S. (1981). Teleconnections in the geopotential height field during the Northern Hemisphere winter. *Monthly Weather Review*, *109*(4), 784–812. https://doi.org/10.1175/1520-0493(1981)109<0784:TITGHF>2.0.CO;2

Wallace, J. M., Smith, C., & Bretherton, C. S. (1992). Singular value decomposition of wintertime sea surface temperature and 500-mb height anomalies. *Journal of climate*, *5*(6), 561–576. https://doi.org/10.1175/1520-0442(1992)005<0561:SVDOWS>2.0.CO;2

Wu, T.-W., & Qian, Z.-A. (2003). The relation between the Tibetan winter snow and the Asian summer monsoon and rainfall: An observational investigation. *Journal of Climate*, *16*(12), 2038–2051. https://doi.org/10.1175/1520-0442(2003)016<2038:TRBTTW>2.0.CO;2

Wu, Q., & Zhang, X. (2010). Observed forcing-feedback processes between Northern Hemisphere atmospheric circulation and Arctic sea ice coverage. *Journal of Geophysical Research*, *115*, D14119. https://doi.org/10.1029/2009JD013574

Xiao, Z., & Duan, A. (2016). Impacts of Tibetan Plateau snow cover on the interannual variability of the East Asian summer monsoon. *Journal of Climate*, *29*(23), 8495–8514. https://doi.org/10.1175/JCLI-D-16-0029.1

Xiao, B., Zhang, Y., Yang, X.-Q., & Nie, Y. (2016). On the role of extratropical air-sea interaction in the persistence of the Southern Annular Mode. *Geophysical Research Letters*, *43*, 8806–8814. https://doi.org/10.1002/2016GL070255

Xue, Y., De Sales, F., Lau, W. K.-M., Boone, A., Kim, K.-M., Mechoso, C. R., et al. (2016). West african monsoon decadal variability and surface-related forcings: Second West African monsoon modeling and evaluation project experiment (WAMME II). *Climate Dynamics*, *47*(11), 3517–3545. https://doi.org/10.1007/s00382-016-3224-2

Xue, Y., Diallo, I., Li, W., David Neelin, J., Chu, P. C., Vasic, R., et al. (2018). Spring land surface and subsurface temperature anomalies and subsequent downstream late spring-summer droughts/floods in North America and East Asia. *Journal of Geophysical Research: Atmospheres*, *123*, 5001–5019. https://doi.org/10.1029/2017JD028246

Xue, Y., Ji, J., Sun, S., Wu, G., Lau, K.-M., Poccard, I., et al. (2005). Multiscale variability of the river runoff system in China and its long-term link to precipitation and sea surface temperature. *Journal of Hydrometeorology*, *6*(4), 550–570. https://doi.org/10.1175/JHM439.1

Xue, Y., Oaida, C. M., Diallo, I., Neelin, J. D., Li, S., De Sales, F., et al. (2016). Spring land temperature anomalies in northwestern US and the summer drought over Southern Plains and adjacent areas. *Environmental Research Letters*, *11*(4), 044018. https://doi.org/10.1088/1748-9326/11/4/044018

Xue, Y., Vasic, R., Janjic, Z., Liu, Y., & Chu, P. C. (2012). The impact of spring subsurface soil temperature anomaly in the western US on North American summer precipitation: A case study using regional climate model downscaling. *Journal of Geophysical Research*, *117*, D11103. https://doi.org/10.1029/2012JD017692

Yasunari, T., Kitoh, A., & Tokioka, T. (1991). Local and remote responses to excessive snow mass over Eurasia appearing in the northern spring and summer climate. *Journal of the Meteorological Society of Japan Series II*, *69*(4), 473–487. https://doi.org/10.2151/jmsj1965.69.4_473

Yatagai, A., Kamiguchi, K., Arakawa, O., Hamada, A., Yasutomi, N., & Kitoh, A. (2012). APHRODITE: Constructing a long-term daily gridded precipitation dataset for Asia based on a dense network of rain gauges. *Bulletin of the American Meteorological Society*, *93*(9), 1401–1415. https://doi.org/10.1175/BAMS-D-11-00122.1

Yuan, C., Li, W., Guan, Z., & Yamagata, T. (2018). Impacts of April snow cover extent over Tibetan Plateau and the central Eurasia on Indian Ocean Dipole. *International Journal of Climatology*. https://doi.org/10.1002/joc.5888

Yuan, C., Tozuka, T., Miyasaka, T., & Yamagata, T. (2009). Respective influences of IOD and ENSO on the Tibetan snow cover in early winter. *Climate dynamics*, *33*(4), 509–520. https://doi.org/10.1007/s00382-008-0495-2

Yuan, C., Tozuka, T., & Yamagata, T. (2012). IOD influence on the early winter Tibetan Plateau snow cover: Diagnostic analyses and an AGCM simulation. *Climate dynamics*, *39*(7-8), 1643–1660. https://doi.org/10.1007/s00382-011-1204-0

Zhang, Y., Yang, X.-Q., Nie, Y., & Chen, G. (2012). Annular mode-like variation in a multilayer quasigeostrophic model. *Journal of the Atmospheric Sciences*, *69*(10), 2940–2958. https://doi.org/10.1175/JAS-D-11-0214.1

Zhang, L., & Zhou, T. (2015). Drought over East Asia: A review. *Journal of Climate*, *28*(8), 3375–3399. https://doi.org/10.1175/JCLI-D-14-00259.1

Zhao, P., Zhou, Z., & Liu, J. (2007). Variability of Tibetan spring snow and its associations with the hemispheric extratropical circulation and East Asian summer monsoon rainfall: An observational investigation. *Journal of Climate*, *20*, 3942–3955. https://doi.org/10.1175/JCLI4205.1